Simultaneous Lidar Observations of an Noctilucent Cloud and an Internal Wave in the Polar Mesosphere

R. Collins[1], M. C. Kelley[2], M. J. Nicolls[2], C. Ramos[2], T. Hou[1], T. E. Stern[3], K. Mizutani[4] and T. Itabe[4].

Abstract. Lidar and radar observations of the upper mesosphere and lower thermosphere were conducted in interior Alaska (65° N, 147° W) during the summer of 2001. Lidar observations of a noctilucent cloud (NLC) were made on the night of 20-21 August 2001 during a visible noctilucent cloud display when the midnight solar depression angle was 12°. These nighttime lidar observations in late August have yielded measurements of both the NLC at 82.7 km and the mesospheric temperature profile below the cloud (~40-80 km). Analysis of the temperature profile indicates the presence of a wave with a vertical wavelength of 7.9 km. The altitude of the NLC coincides with the negative temperature phase of the wave. Located approximately 50 km from the lidar, the radar observations yielded measurements of Polar Mesosphere Summer Echoes (PMSEs) during daytime on 21 August 2001. The PMSE layer occurs just above the NLC layer and also shows structural characteristics associated with the passage of gravity waves through the layer. The presence of NLCs in late August supports recent reports that the late summer Arctic mesosphere is colder and wetter than represented in 'standard' models. These NLC observations are discussed in terms of earlier lidar observations over Alaska, observations at other sites, and current models.

[1] Geophysical Institute and Department of Electrical and Computer Engineering, University of Alaska Fairbanks, Fairbanks, AK 99775, USA.
[2] School of Electrical and Computer Engineering, Cornell University, Ithaca, NY 14853, USA.
[3] Geophysical Institute and Department of Physics, University of Alaska Fairbanks, Fairbanks, AK 99775, USA.
[4] Applied Research and Standards Division, Communications Research Laboratory, 4-2-1 Nukui-kita, Koganei, Tokyo 184-8795, Japan.

1. Introduction

The summer mesopause region (~80-100 km) is of particular interest as transport processes maintain temperatures as low as 120 K during the summer [*Philbrick et al*., 1984; *Schmidlin*, 1992]. Currently we do not understand how small-scale dynamics drive the summertime transport that yields these cold summertime temperatures [*McIntyre*, 1989]. These cold summer temperatures allow the formation of noctilucent clouds (NLCs) in the polar summer. NLCs (also termed polar mesospheric clouds) are formed of small water ice particles [*von Cossart et al*., 1999; *Hervig et al.*, 2001]. NLCs were first reported in the scientific literature in the late 19th century [*Backhouse*, 1885]. These clouds appear to have increased in frequency in the 20th century [*Gadsden and Schröder*, 1989]. Models of the middle atmosphere indicate that the summer mesosphere should get colder as increases in carbon dioxide and methane concentrations yield a colder middle atmosphere [*Roble and Dickinson*, 1989]. Based on these studies researchers have suggested that the polar summer mesosphere will become cloudier as more NLCs form (see *Thomas* [1997; 1996; 1991], and references therein). This cloudy mesosphere scenario has prompted much of the current research effort in studying NLCs as a fingerprint of global change. However, this global change thesis is controversial as it is not clear how changes in the radiative heating budget will effect a region of the atmosphere that is currently maintained far from radiative equilibrium. Only recently have routine lidar measurements of NLCs been established at polar sites (e.g. Scandinavia, [e.g. *von Zahn et al*. 1998; 2000], Greenland, [*Gerrard et al*., 1998; *Thayer et al.*, 1995], and Antarctica [*Chu et al*., 2001]). Different theories of NLC formation yield size distributions in agreement with recent three-color lidar measurements [*von Cossart et al*., 1999]. Observational studies are limited by the seasonal occurrence (late-June to mid-August) of these clouds and their spatial and temporal patchiness. Furthermore, high-resolution measurements of the temperatures and winds in this region are uncommon [*Lübken*, 1999]. Polar Summer Mesosphere Echoes (PMSEs) (see review by Cho and Röttger, [1997] and references therein) are associated with NLCs. PMSEs are understood to

be the radio echoes from charged subvisible aerosols near the mesopause that grow and sediment downwards forming the visible NLCs.

Fogle and coworkers developed a network for the observation of NLCs in North America during a four-year study that began in 1962 [*Fogle* 1966; *Fogle and Haurwitz*; 1966]. As part of that effort they attempted to make lidar measurements in Fairbanks, Alaska during the summer of 1964 but were unsuccessful due to overcast conditions that summer. PMSE were first reported in VHF radar measurements made with the Poker Flat MST radar at Chatanika [*Ecklund and Balsley*; 1981]. The MST radar operated from 1979 until 1985. The radar data has been used to study PMSE nucleation processes [*Sugiyama et al*., 1996] and seasonal variations of PMSE with temperature [*Balsley and Huaman*, 1997]. The Communications Research Laboratory (CRL) Rayleigh Lidar was installed at Poker Flat Research Range, Chatanika, Alaska (65°N, 147°W) in November 1997. CRL and the Geophysical Institute of the University of Alaska Fairbanks jointly operate the CRL Rayleigh lidar. The lidar observations were made during nighttime under clear skies between August and April. NLCs have been detected on four occasions during the month of August. In the summer of 2001 lidar observations were conducted in cooperation with radar measurements at the High Power Auroral Stimulation (HIPAS) Observatory at Two Rivers, Alaska. HIPAS observatory is located 50 km SE of the lidar site. The University of California at Los Angeles (UCLA) operates the HIPAS observatory. Cornell University researchers conducted the radar measurements with support from UCLA. In this study we focus on lidar observations from the night of August 20-21 and the radar observations from midday of 21 August 2001. In late August the nighttime solar depression angle was low enough (> 12° below the horizon) to yield lidar measurements of both an NLC at 82.7 km and the mesospheric temperature profile (~40-80 km). We characterize NLCs in terms of backscatter ratio, altitude and width. We compare the observed characteristics with those of the PMSE measured by the radar.

2. Experiment and Methods

The CRL Rayleigh lidar system consists of a Nd:YAG laser, a 0.6 m receiving telescope, a photomultiplier tube, a photon counting detection system, and a computer-based data acquisition system [*Mizutani et al*., 2000]. The lidar is a fixed zenith-pointing system. The laser operates at 532 nm with a pulse repetition rate of 20 pps. The laser pulse width is 7 ns FWHM, and the average laser power is 10W. The field-of-view of the receiver telescope is 1 mrad and the optical bandwidth 1 nm FWHM. The photon counts are integrated over 0.5 μsec yielding a 75 m range sampling resolution. The photon count profile is smoothed with a running average over 2 km before the data is further processed. The NLC backscatter ratios are determined by interpolating the lidar signal across the altitude of the cloud layer between altitudes where the lidar signal is dominated by Rayleigh scatter. A statistically significant cloud echo is detected when the difference between the lidar signal at the peak of the NLC and the interpolated Rayleigh lidar signal at that altitude is greater than the sum of the associated photon count errors. An NLC is detected if it is identified as significant feature in the lidar signal profile. The lidar profile for a 20-min observation period on the night of 4-5 August 1999 is shown in Figure 1. Following *von Zahn and Bremer* [1999] we present the lidar data normalized to one at a given altitude (i.e. 70 km). The NLC echo is clearly visible with a maximum at 82.2 km. The Rayleigh lidar technique assumes that the intensity profile of the scattered light is proportional to the density of the atmosphere, and that the atmosphere is in hydrostatic equilibrium.

The temperature profiles are determined from the photon count profiles under standard inversion techniques (e.g. *Leblanc et al*., [1998]). The initial temperature at the upper altitude (80 km) is chosen from the study by *Lübken* [1999]. *Lübken* reported a data set of mesospheric temperature profiles based on 89 falling sphere experiments made over a 10-yr period. The falling sphere data set has shown that the mesopause is colder in late August than suggested by the MSISE90 model [*Hedin*, 1991]. During astronomically-dark clear-sky conditions the Rayleigh lidar measurements yield temperature profiles at 2 h intervals [*Cutler et al.*, 2001]. Waves in the lidar Rayleigh lidar profile are determined in a two step process. The temperature profile is smoothed with a running average over 6 km and a third order spline is fit to the

temperature profile. A density profile is calculated from the spline temperature profile under the assumption of hydrostatic equilibrium. The initial density at the lowest altitude (40 km) is chosen from *Lübken* [1999]. This spline density profile is assumed to represent the background density profile. The relative density perturbation is then calculated as the relative difference between the spline density profile and the range scaled lidar signal profile.

The HIPAS Observatory has a high power HF transmitter with an effective radiated power of nearly 100 megawatts [*Wong et al*., 1990]. A variety of waveforms can be transmitted over the frequency range from 3-5 MHz. In this study the radar system consisted of the main multiple dipole antenna system that transmitted the radio waves and an ionosonde antenna that received them. The radar operated at 4.53 MHz and probed the 80 to 90 km altitude region with a height resolution of 2 km. The radar is sensitive to PMSE formations and the observations yielded a PMSE profile every 10 minutes. The radar measurements are presented as signal-to-noise-ratio (SNR) profiles that are calculated from the radar echoes. All times in the paper are given in local standard time (LST = UT-9 h).

3. Observations

On the night of 20-21 August 2001 the sun set at 2048 LST and rose at 0501 LST. The sun was greater than 6° below the horizon from 2153 until 0355 LST, and 12° or more below the horizon from 2345 until 0206 LST [*USNO*, 2002]. The staff on-site video recorded an NLC display in the NE from about 2311 LST that persisted until early morning. A statistically significant NLC echo was detected in the integrated lidar profile from 2217 until 2242 LST. The lidar signal profile is plotted in Figure 2. A weak NLC echo is clearly observed with a peak backscatter ratio of 1.4 at 82.7 and an altitude extent (where the backscatter ratio is greater than unity) of 2.6 km. These characteristics are typical of previous lidar measurements of NLCs in August at PFRR (Table 1). Visual displays of NLCs have been observed by the staff onsite during each of the nights when these lidar measurements were conducted. The visual NLC displays have the classic characteristics of NLC displays [*Fogle*, 1966]; the displays can persist

for periods of several hours, the displays show well-defined wave structure, and the displays appear before midnight but are brightest and most extensive after midnight.

The average temperature profile for the darkest part of the observation period (2216 20 August – 0316 21 August) is plotted in Figure 3. The MSISE90 [*Hedin*, 1991] profile for local midnight on the night of August 20-21 and the late August falling sphere temperature profile of *Lübken* [1999] (termed L99) are also plotted for comparison. The lidar data and the L99 profile have the same temperature at the seed temperature altitude of 80 km. However, the lidar temperature profile remains in agreement with the L99 profile down to 70 km, indicating that the similarity in upper mesosphere temperatures is not just due to the agreement in the seed temperature. The MSISE90 temperature profile is 10 K warmer than the other profiles at 80 km and is 13 K warmer than the L99 profile at the mesopause. Combining the temperature and relative density profile measured by the Rayleigh lidar we find an oscillation in the density data between 55 and 75 km (Figure 4). This oscillation has a period of 7.9 km and a growth length of 15.6 km. Using the gravity wave polarization and dispersion relations [*Hines*, 1960] we determine the temperature characteristics of the wave assuming that the period of the wave is greater than 6 h. For these long-period waves the phase relationship between density and temperature fluctuations is insensitive to period. The altitude of the NLC is in the negative phase of the wave. The amplitude of the wave is 3.4 K at the altitude of the NLC. The estimated amplitude of the wave component is smaller than the actual amplitude as the photon count profile is smoothed over 2 km and integrated over 5 h. We expect that the actual amplitude may be at least twice as large as our estimate.

The radar measurements were made on the afternoon of 21 August from 1230 to 1400 LST. The sequence of SNR profiles is plotted in Figure 5. Each SNR profile represents a 3 minute integrated measurement made every 10 minutes. The average PMSE profile (Figure 6) shows scattering at 82 km that increases significantly starting at 85 km and reaches a maximum at 90 km. The altitude distribution of the PMSE and NLC is similar to that reported in simultaneous and common-volume lidar and radar observations at ALOMAR (69°N, 14°E) (see Figures 1.b,

2b, 3b of *von Zahn and Bremer* [1999]). Similar to *von Zahn and Bremer* we note that the NLC layer is considerably narrower than the PMSE layer and the lower edges of the NLC and PMSE layer coincide. Figure 5 also shows a downward phase progression in the PMSE profiles. These downward phase progressions are a common characteristic of NLC and PMSE observations and are understood to represent the passage of upwardly propagating gravity waves through the PMSE layer [*Cho and Röttger*, 1997].

4. Discussion

The NLC layer was observed on the night of 20-21 August and the PMSE layer was detected during the day on August 21 suggesting that the conditions in the mesopause region remained relatively stable during this period. Seasonal studies of NLCs have shown that the occurrence of NLCs in the northern hemisphere drops off dramatically during August and that an NLC observation this late in the summer is relatively unusual [e.g. *Fogle*, 1966*; Gadsden and Schröder*, 1989].

Given the recent set of falling sphere temperature measurements [*Lübken*, 1999] and discovery of a mesospheric water vapor layer [*Summers et al.*, 2001] we discuss these observations in terms of the thermal structure and water vapor distribution in the mesopause region. *Marti and Mauersberger* [1993] determined the following relationship for the vapor pressure over ice in the temperature range 170 K to 250 K,

$$\log_{10}(p_{SAT}) = 12.537 - (2663.5/T) \qquad (1)$$

where p_{SAT} is the saturation vapor pressure (pa) and T is the temperature (K). The degree of saturation is then given by $S = p_{WATER}/p_{SAT}$, where p_{WATER} is the partial pressure of water vapor. If S is greater than 1 the air is supersaturated, and we expect ice particles to grow. If S is less than 1 we expect that the ice particles will sublimate. Using density and temperature profiles we determine the saturation vapor pressure and hence the saturation mixing ratio as a function of altitude. Recent space-based observations have revealed the presence of a narrow water layer centered between 82 and 84 km during the Arctic summer [*Summers et al.*, 2001]. The mixing

ratios at the peak of the layer are 10-15 ppmv. Subsequent studies have detected a region of enhanced water vapor poleward of 65°N during mid-August in the northern hemisphere [*Stevens et al.*, 2001]. The mixing ratios vary considerably from 3 ppmv to 23 ppmv with an average value of 12 ppmv. These water vapor mixing ratios are larger than previously accepted (~ 2ppmv).

We consider the water vapor pressure required to allow ice crystals to form under four different scenarios; the atmosphere defined by MSISE90, the atmosphere reported by of *Lübken* [1999] (L99), L99 with a small wave-induced decrease (= 3.4 K at 82 km, as determined from the harmonic fit to the lidar data), and L99 with a doubled small wave-induced decrease (6.8 K at 82 km). The calculated saturation water vapor mixing ratio profiles for these four cases are plotted in Figure 6. The values of the saturation water vapor mixing ratio at 82 km, 83 km and 88 km (corresponding to the mesopause) are presented in Table 2. From Figure 6 and Table 2 we see that in the MSISE model (thick line with square bullets) would require an unrealistically high ambient water concentration for NLCs to form. The pair of vertical dashed lines mark the maximum (23 ppmv) and minimum (3ppmv) water vapor mixing ratios reported by Stevens et al. [2001]. L99 (thick line) supports formation of ice crystals between 84 km and 90 km for water vapor mixing ratios of 23 ppmv. The water vapor mixing ratio would have to be in the range 40-88 ppmv for an NLC to form at 82.7 km. The third scenario (thick long-dashed line), L99 with the wave-induced temperature decrease, supports ice crystal formation from 83 km to 91 km for water vapor mixing ratios of 23 ppmv. The water vapor mixing ratio would have to be in the range 17-40 ppmv for an NLC to form at 82.7 km. The last scenario (thick short-dashed line), L99 with the doubled wave-induced temperature decrease, supports ice crystal formation from 82 km to 93 km for water vapor mixing ratios in the range ppmv. The water vapor mixing ratio would have to be in the range 6.5-17 ppmv for an NLC to form at 82.7 km. The water vapor mixing ratios of 10-15 ppmv reported by Summers et al. [2001] at 82-84 km would support the formation of the observed NLC under these conditions. From these calculations we conclude that the ambient partial pressure of water vapor is between 7 and 17 ppmv at 82.7 km.

Warren and coworkers [*Warren et al.*, 1997] discussed the observation of an NLC display in May at the South Pole. In discussing this unusual event, the authors noted that NLCs have been reported more often in warmer temperatures at the end of the summer season than at the start of the season. This observation is consistent with the conclusion of Summers and coworkers [*Summers et al*., 2001] that the polar summer mesospheric region accumulates water vapor over the course of the summer through upwelling from below. Recent studies of particle charging in the polar summer mesosphere show that observed PMSE characteristics are consistent with water vapor concentrations of 4-14 ppmv which is again larger than 'standard' *values [Lübken and Rapp*, 2001].

5. Summary and Conclusions

We have measured a weak NLC layer with a Rayleigh lidar in late August near local midnight. A visual NLC display was recorded on the same night and a PMSE layer was measured by radar near noon of the following day. The Rayleigh lidar measurements also yielded measurements of the temperature profile below the NLC. The temperature observations are consistent with the thermal structure of the Arctic summer mesosphere reported by *Lübken* [1999] that is colder than 'standard' models. The lidar also detected the presence of an internal wave. Wave activity is also observed in the PMSE profiles measured by the radar. Even in the presence of gravity waves which modulate the environment, these observations suggest that the amount of water vapor in the Arctic summer mesosphere is higher (~7-17 ppmv) than 'standard' models assume (~2ppmv). Like *Lübken*, we note that the observations cannot be explained in terms of the MSISE90 model and serve as a caution to studies that employ the standard empirical models to determine relationships between NLCs and the thermal structure of the polar summer mesosphere. The NLC observations are consistent with the recent discovery of a water vapor enhancement in the summer polar mesosphere [*Summers et al*., 2001; *Stevens et al*., 2001].

Acknowledgments. The authors thank the staff at Poker Flat Research Range and the High Power Auroral Stimulation Observatory for their support. The authors particularly thank Eric Nichols and Al Wong for their assistance during the radar experiment and Joaquin Vieira and Kevin Rasmussen for their assistance during the lidar experiment. The observations of 20-21 August were conducted in cooperation with the Polar Aeronomy and Radio Science Summer School. The authors acknowledge the support of the Communication Research Laboratory and the support from the Office of Naval Research under grants N00014-00-1-0658 and N00014-01-1-0104. Poker Flat Research Range is a rocket range operated by the Geophysical Institute of the University of Alaska Fairbanks under contract from NASA.

References

Balsley, B. B., and M. Huaman, On the relationship between seasonal occurrence of northern hemispheric polar mesosphere summer echoes and mean mesopause temperature, *J. Geophys. Res*., 102, 2021-2024, 1997.

Backhouse, T. W., The luminous cirrus cloud of June and July, *Meteorol. Mag*., 20, 133, 1885.

Cho, J. Y. N., and J. Röttger, An updated review of polar mesosphere summer echoes: Observation, theory, and their relationship to noctilucent clouds and subvisible aerosols, *J. Geophys. Res*., 102, 2001-2020, 1997.

Chu, X., C. S. Gardner, and G. Papen, Lidar observations of polar mesospheric cloud at the South Pole: Seasonal variations, *Geophys. Res. Lett*., *28*, 1203-1207, 2001.

Cutler, L. J., R. L. Collins, K. Mizutani, and T. Itabe, Rayleigh Lidar Observations of Mesospheric Inversion Layers at Poker Flat, Alaska 67 °N, 147° W, *Geophys. Res. Lett.*, *28*, 1467-1470, 2001.

von Cossart, G. J. Fiedler, U. von Zahn, Size distribution of NLC particles as determined from three-color observations of NLC by groundbased lidar, *Geophys. Res. Lett.*, *26*, 1513-1516, 1999.

Ecklund, W. L., and B. B. Balsley, Long-term observations of the Arctic mesosphere with the MST radar at Poker Flat, Alaska, *J. Geophys. Res., 86*, 7775-7780, 1981.

Fogle, B. T., *Noctilucent Clouds*, Ph.D. Dissertation, University of Alaska Fairbanks, pp156, 1966.

Fogle, B. and B. Haurwitz, Noctilucent Clouds, Space Sci. Rev., 6, 281-340, 1966.

Gadsden, M., and W. Schröder, *Noctilucent Clouds*, Springer-Verlag, Berlin, pp165, 1989.

Gerrard, A. J., Kane, T. J., and J. P. Thayer, Noctilucent clouds and wave dynamics: Observations at Sondestrom, Greenland, *Geophys. Res. Lett.*, *25*, 2817-2820, 1998.

Hedin, A. E., Extension of the MSIS thermospheric model into the middle and lower atmosphere, *J. Geophys. Res.*, *96*, 1159, 1991.

Hervig, M., R. E. Thompson, M. McHugh, L. L. Gordley, J. M. Russell III, M. E. Summers, First confirmation that water ice is the primary component of polar mesospheric clouds, *Geophys. Res. Lett., 28*, 971-974, 2001.

Hines, C.O., Internal atmospheric gravity waves at ionospheric heights, *Can. J. Phys., 38*, 1441-1481, 1960.

Leblanc, T., I. S. McDermid, A. Hauchecorne, and P. Keckhut, Evaluation of optimization of lidar temperature analysis algorithms using simulated data, *J. Geophys. Res., 103*, 6177-6187, 1998.

Lübken, F. -J , and M. Rapp, Modelling of particle charging in the polar summer mesosphere: part 2 – Application to measurements, *J. Atmos. Solar-Terr. Phys., 63*, 771-780, 2001.

Lübken, F. -J., Thermal structure of the Arctic summer mesosphere, *J. Geophys. Res., 104*, 9135-9149, 1999.

Marti, J., and K. Mauersberger, A survey and new measurements of ice vapor pressure at temperature between 170 and 250K, , *Geophys. Res. Lett., 20*, 363-366, 1993.

McIntyre, M. E., On dynamics and transport near the polar mesopause in summer, *J. Geophys. Res., 94*, 14617-14628, 1989.

Mizutani, K., T. Itabe, M. Yasui, T. Aoki, Y. Murayama, R. L. Collins, Rayleigh and Rayleigh Doppler Lidars for the Observations of the Arctic Middle Atmosphere, *IEICE Trans. Comms., E83-B*, 2003, 2000.

Philbrick, C. R., J. Barnet, R. Gerndt, D. Offermann, W. R. Pendleton Jr., P. Schylter, J. F. Schmidlin, and G. Witt, Temperature measurements during the CAMP campaign, *Adv. Space Res.* 4, 153-156, 1984.

Roble, R. G., and R. E. Dickinson, How will changes in carbon dioxide and methane modify the mean temperature structure of the mesosphere and thermosphere, *Geophys. Res. Lett., 16*, 1441-1444, 1989.

Schmidlin, F. J., First observations of mesopause temperatures lower than 100 K, *Geophys. Res. Lett.*, 1643-1647, 1992.

Stevens, M. H., R. R. Conway, C. R., Englert, M. E. Summers, K. U. Grossmann, and O. A. Gusev, PMCs and the water frost point in the Arctic summer mesosphere, *Geophys. Res. Lett., 28*, 4449-4452, 2001.

Sugiyama, T., Y. Muraoka, H. Sogawa, and S. Fukao, Oscillations in polar mesospheric echoes and bifurcation of noctilucent cloud formation, *Geophys. Res. Lett.*, 23, 653-656, 1996.

Summers, M. E., R. R. Conway, C. R. Englert, D. E. Siskind, M. H. Stevens, J. M. Russell III, L. L. Gordley, and M. J. McHugh, Discovery of a Water Vapor Layer in the Arctic Summer mesosphere: Implications for Polar Mesospheric Clouds, *Geophys. Res. Lett., 28*, 3601-3604, 2001.

Thayer, J. P., N. Nielsen, and J. Jacobsen, Noctilucent cloud observations over Greenland by a Rayleigh lidar, *Geophys. Res. Lett., 22*, 2961-2964, 1995.

Thomas, G. E., Noctilucent cloud workshop, *J. Geophys. Res., 102*, 1957-1958, 1997.

Thomas, G. E., Is the polar mesosphere the miner's canary of global change,*Adv. Spa. Res., 18*, 149-158, 1996.

Thomas, G. E., Mesospheric clouds and the physics of the mesopause region, *Rev. of Geophys., 29*, 553-575, 1991.

US Naval Observatory (USNO), Sun or Moon Altitude/Azimuth Table for One Day, http://aa.usno.navy.mil/data/docs/AltAz.html, accessed April, 2002.

Warren, S. G., G. E. Thomas, G. Hernandez, and R. W. Smith, Noctilucent cloud observed in late April at South Pole Station: Temperature anomaly or meteoric debris ?, *J. Geophys. Res*., *102*, 1991-2000, 1997.

Wong. A. Y., J. Carroll, R. Dickman, W. Harrison, W. Huhn, B. Lum, M. McCarrick, J. Santoru, G. Schock, G. Wong, and R. F. Weurker, High-power radiating facility at the HIPAS observatory, *Radio Sci*., *25*, 1269-1282, 1990.

von Zahn, U., G. von Cossart, J. Fiedler, K. H. Frike, G. Nelke, G. Baumgarten, D. Rees, A. Hauchecorne, and K. Adolfsen, the ALOMAR Rayleigh/Mie/Raman lidar: objectives configuration and performance, Ann. Geophysicae, 18, 815-833, 2000.

von Zahn, U., G. and J. Bremer, Simultaneous and common-volume observations of noctilucent cloud and polar mesosphere summer echoes, *Geophys. Res. Lett.*, *26*, 1521-1524, 1999.

von Zahn, U., G. von Cossart, J. Fiedler and D. Rees, Tidal variations of noctilucent clouds measured at 69°N latitude by groundbased lidar, *Geophys. Res. Lett.*, *25*, 1289-1291, 1998.

Table 1. Characteristics of NLCs observed at Poker Flat Research Range (65N, 147°W)

Date	Time	Altitude (km)	Backscatter Ratio	Width (km)	Solar depression angle(°)
13/08/1998	0042-0054	83.1	1.8	2.6	11 –11
03/08/1999	0110-0135	84.8	2.2	2.3	8 - 8
05/08/1999	0123-0243	82.2	2.6	3.4	8 - 6
20/08/2001	2217-2242	82.7	1.4	2.6	8 - 10

Table 2. Saturation Vapor Pressure of Water

Altitude (km)	MSISE90		L99[1]		$\|T'\|^2$		$2\times\|T'\|^3$	
	Temp. (K)	p_{WATER} (ppm)	Temp. (K)	p_{WATER} (ppm)	Temp. (K)	p_{WATER} (ppm)	Temp. (K)	p_{WATER} (ppm)
82	170	923	159	88	3.2	40	6.4	17
83	166	562	155	40	3.4	17	6.8	6.5
88	158	223	145	7.9	4.7	1.9	9.4	0.4

1. L99 denotes *Lübken* [1999] as source of atmospheric temperature and density data.
2. Temperature is sum of L99 and wave amplitude of |T'|. Temp. shows wave amplitude.
3. Temperature is sum of L99 and wave amplitude of 2×|T'|. Temp. shows wave amplitude.

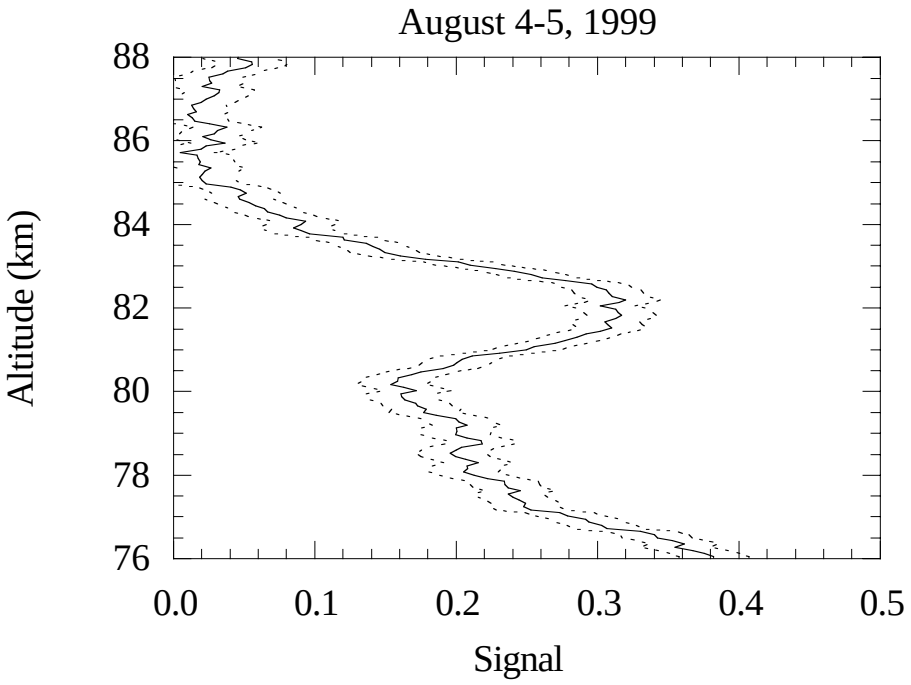

Figure 1. Lidar signal plotted against altitude. The lidar signal is normalized to unity at 70 km. The dashed lines are the one sigma uncertainties about the mean profile. An NLC is clearly observed at 82.2 km.

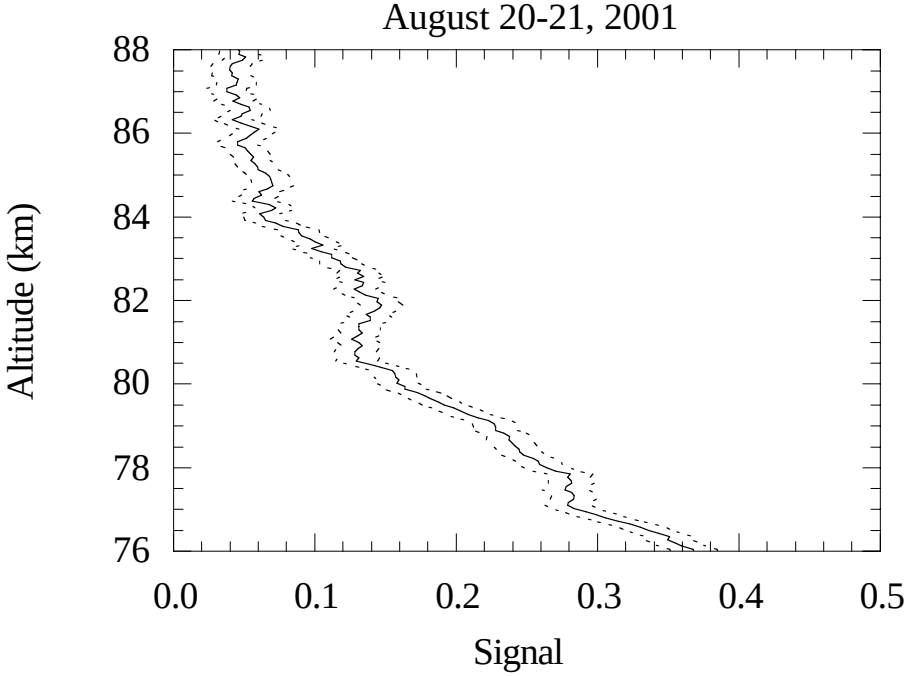

Figure 2. Lidar signal plotted against altitude. The lidar signal is normalized to unity at 70 km. The dashed lines are the one sigma uncertainties about the mean profile. A weak NLC is observed at 82.7 km.

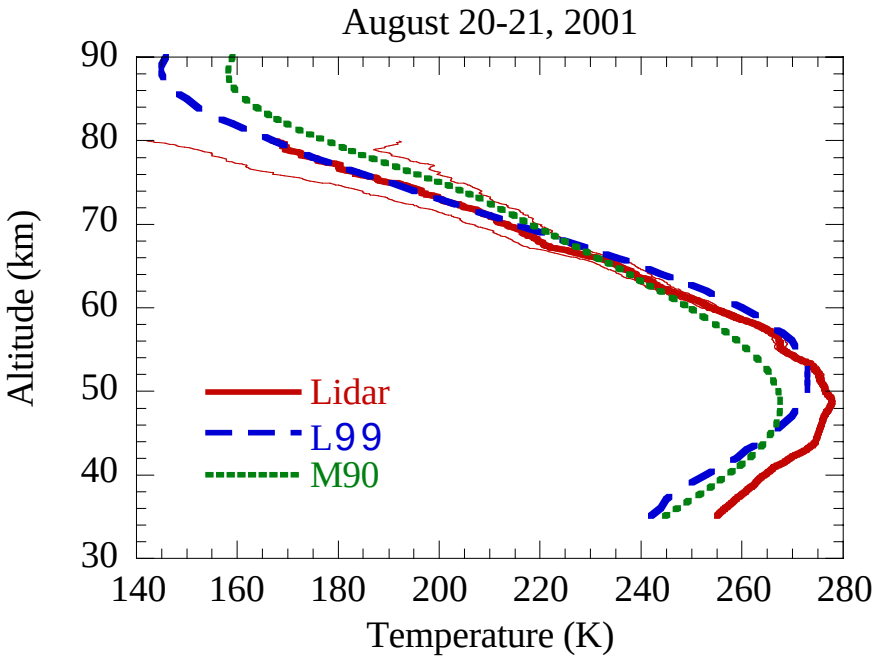

Figure 3. Temperature profiles plotted against altitude. The thick solid line is the lidar measurement (Lidar). The long dashed line is from Lübken [1999] (L99). The short dashed line is from MSISE90 (M90). The thin solid lines are the one sigma uncertainties in the lidar measurement.

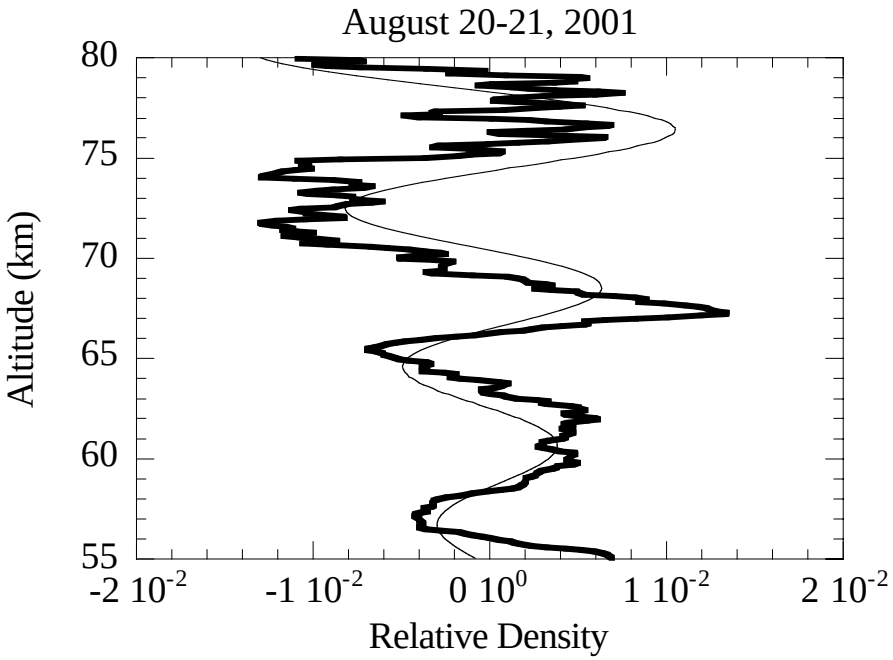

Figure 4. Relative perturbation profile determined from lidar data (thick) plotted against altitude. The harmonic fit to the profile is superimposed(thin).

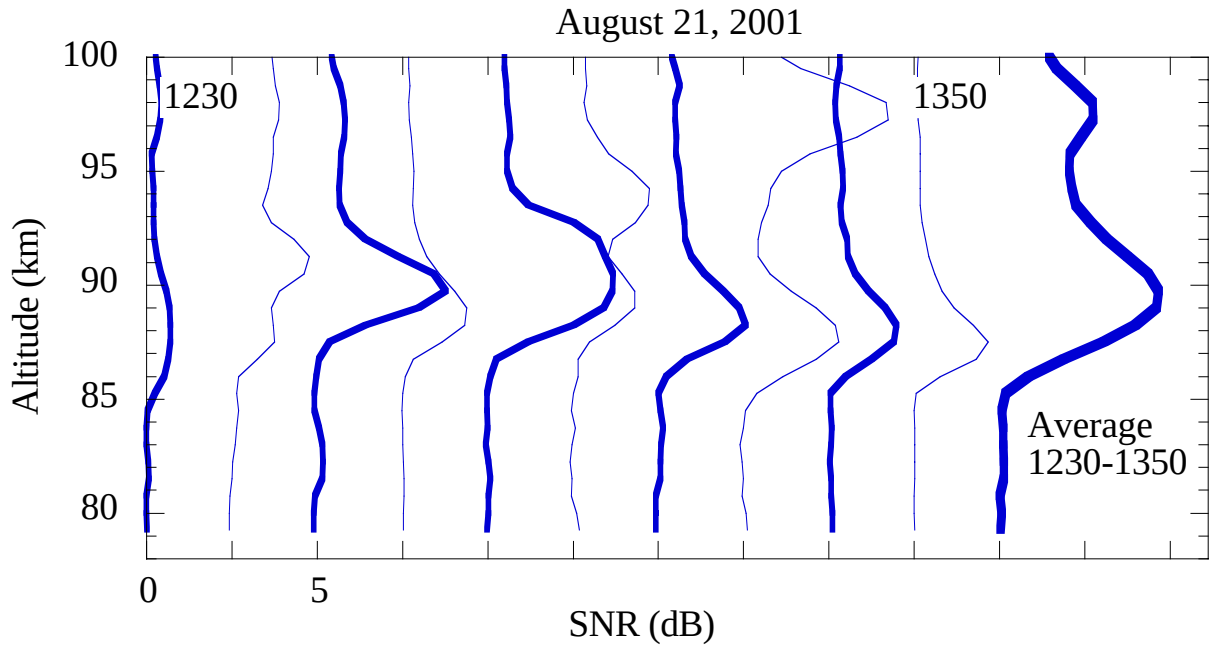

Figure 5. Sequence of PMSE SNR profiles plotted against altitude. The profiles each represent a three-minute measurement and are taken every 10 minutes. The profiles are offset by 2.25. The average profile for the observation period is plotted on the right.

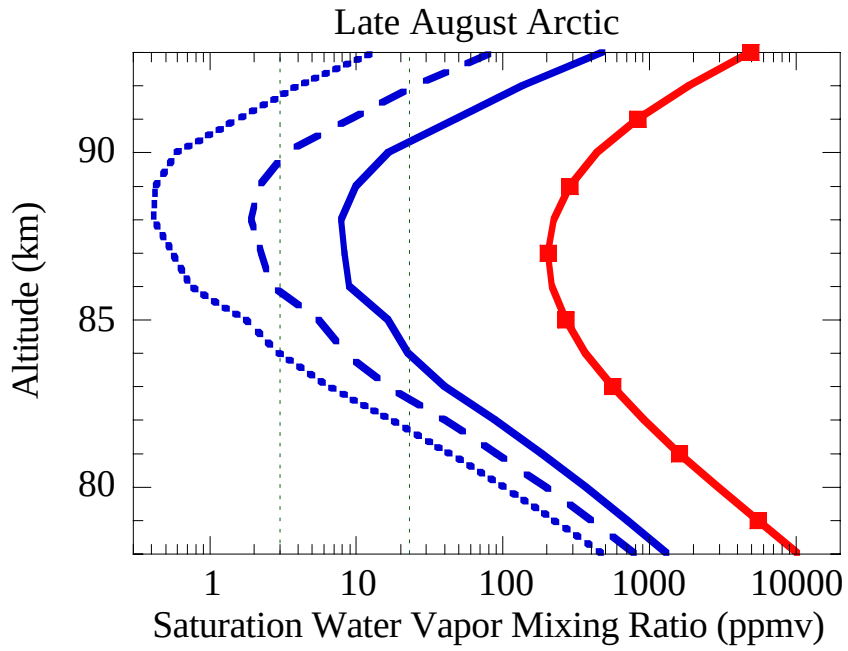

Figure 6. Profiles of saturation water vapor pressure plotted against altitude. The bold solid profile with square bullets is derived from MSIS90. The sold profile is derived from *Lübken* [1999]. The dashed lines are based on the data from Lübken but also include the effect of waves. See text for details. The vertical dashed lines represent the range of water vapor concentrations reported by *Stevens, et al.* [2001].